GW quasiparticle band structures of stibnite, antimonselite, bismuthinite, and guanajuatite

Marina R. Filip, Christopher E. Patrick, and Feliciano Giustino
Department of Materials, University of Oxford, Parks Road, Oxford OX1 3PH, United Kingdom
(Received 21 January 2013; revised manuscript received 26 April 2013; published 17 May 2013)

We present first-principles calculations of the quasiparticle band structures of four isostructural semiconducting metal chalcogenides A_2B_3 (with A = Sb, Bi and B = S, Se) of the stibnite family within the G_0W_0 approach. We perform extensive convergence tests and identify a sensitivity of the quasiparticle corrections to the structural parameters and to the semicore d electrons. Our calculations indicate that all four chalcogenides exhibit direct band gaps, if we exclude some indirect transitions marginally below the direct gap. Relativistic spin-orbit effects are evaluated for the Kohn-Sham band structures, and included as scissor corrections in the quasiparticle band gaps. Our calculated band gaps are 1.5 eV (Sb_2S_3), 1.3 eV (Sb_2Se_3), 1.4 eV (Bi_2S_3), and 0.9 eV (Bi_2Se_3). By comparing our calculated gaps with the ideal Shockley-Queisser value we find that all four chalcogenides are promising as light sensitizers for nanostructured photovoltaics.

DOI: 10.1103/PhysRevB.87.205125 PACS number(s): 71.20.−b, 74.70.Xa, 78.20.−e, 78.56.−a

I. INTRODUCTION

The development of sustainable energy solutions based on scalable processes and nontoxic materials constitutes a key priority in the current scientific research agenda, and in this area nanostructured energy-harvesting solar and thermoelectric devices are playing a lead role. Recently there has been a surge of interest in devices using semiconducting metal chalcogenides of the stibnite family. For example recent studies have demonstrated the potential of these semiconductors both in photovoltaics applications,[1–4] and in thermoelectric generators.[5]

In the area of nanostructured photovoltaics semiconducting metal chalcogenides have successfully been used to replace the inorganic dye in dye-sensitized solar cells,[6] leading to the development of solid-state semiconductor-sensitized solar cells.[1,7] In these devices thin layers or nanoparticles of the semiconducting chalcogenides act as light absorbers, and upon photoexcitation they transfer an electron to the acceptor (typically TiO_2) and a hole to the hole-transporter (for example a conducting polymer). The record efficiency within this class of devices is 5.1% and was obtained using stibnite (Sb_2S_3) as semiconductor sensitizer.[1]

A recent atomistic computational study of photovoltaic interfaces for semicondictor-sensitized solar cells pointed out that, in addition to stibnite, the other members of the stibnite mineral family, namely antimonselite (Sb_2Se_3), bismuthinite (Bi_2S_3), and guanajuatite (Bi_2Se_3), exhibit optical properties similar to stibnite and should be considered as potential candidates for novel semiconductor sensitizers.[8] Using density-functional calculations and empirical scissor corrections of the band gaps, in Ref. 8 it was found that stibnite and antimonselite should form type-II heterojunctions with TiO_2, while bismuthinite should form a type-I heterojunction and hence would not be able to transfer electrons to TiO_2. These theoretical predictions have recently been confirmed by the experimental investigations of Refs. 4 and 9, thereby providing a motivation for further studies and for the more sophisticated analysis presented in this work.

The four minerals of the stibnite family crystallize in an orthorhombic structure consisting of parallel one-dimensional $(A_4B_6)_n$ ribbons, with A = Sb, Bi and B = S, Se. A ball-and-stick model of this structure is shown in Fig. 1. Besides its natural occurrence in mineral form, stibnite can be synthesized using a variety of low-cost fabrication techniques.[10–18] Using these techniques it is possible to obtain a good degree of crystallinity,[19,20] to control dimensionality,[5,16,21] and to tune the optical properties.[16,22–24] Semiconductors of the stibnite family have also been synthesized in various nanostructured forms. For example Refs. 5,14,15 and Refs. 5,24 reported nanowires and nanotubes, respectively, of stibnite, antimonselite, and bismuthinite. Nanowires of stibnite were found to exhibit enhanced ferroelectric and piezoelectric properties as compared to their bulk counterpart.[25] Nanowires and nanotubes of antimonselite were found to exhibit conductivities much higher than their bulk counterpart,[5] and are being considered for thermoelectric applications. In the case of bismuthinite, Ref. 14 reported nanowires with diameters as small as 1.6 nm, corresponding to a transverse size of only two ribbons. The rhombohedral phase of Bi_2Se_3 has been investigated extensively since this compound is a prototypical topological insulator.[26] However to the best of our knowledge little is known about orthorhombic Bi_2Se_3, i.e., guanajuatite, which is stable only at high temperature and pressure.[27,28]

The band gaps of stibnite, antimonselite, and bismuthinite have been measured extensively via optical absorption experiments. The band gap of stibnite ranges between 1.42–1.78 eV.[29,30] For antimonselite Ref. 31 reported a direct gap of 1.55 eV, while Ref. 32 gave an indirect gap between 1–1.2 eV. The measured band gap of bismuthinite is 1.38–1.58 eV.[33–35] The spread in the measured gaps can be attributed to the different preparation conditions used, yielding different degrees of polycrystallinity and even amorphous samples in some cases, and also different stoichiometries. In addition all these compounds exhibit closely lying direct and indirect transitions (cf. Fig. 3 below), thereby complicating the assignment of the nature of the optical gap.

All four minerals of the stibnite family have been investigated in detail using density-functional theory (DFT) calculations. The electronic properties of these compounds have been studied in Refs. 8 and 36–42, and the elastic and optical properties have been calculated in Ref. 39.

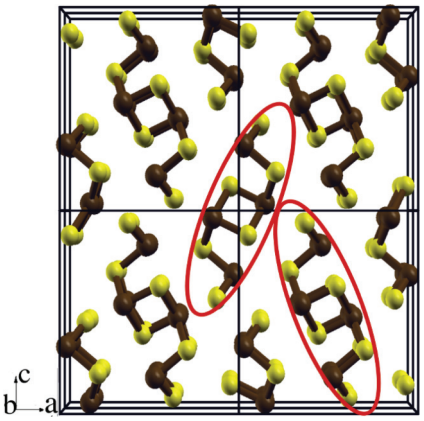

FIG. 1. (Color online) Ball-and-stick model of A_2B_3 semiconducting metal chalcogenides of the stibnite family, with A standing for Sb or Bi (brown), and B for S or Se (yellow). The two inequivalent $(A_4B_6)_n$ ribbons in the unit cell are highlighted in red, and the perspective view is along the direction of the ribbons.

A comparison of the theoretical studies published so far shows some inconsistencies in the calculated band gaps; for example, the values reported for stibnite are in the range 1.18–1.55 eV.[8,36,39,43] As expected all the calculated DFT gaps underestimate the measured band gaps. To the best of our knowledge only one work[43] reported a calculation of the quasiparticle band gap of stibnite and antimonselite within the *GW* approximation.[44] The electronic structure of the rhombohedral Bi_2Se_3 has also been explored within the *GW* approach.[45]

Within this context there exists a need for detailed and reproducible calculations of the electronic structure of stibnite and related compounds based on state-of-the-art quasiparticle techniques. In line with this need the goal of the present work is to report a systematic and reproducible study of the quasiparticle band structures of all four A_2B_3 semiconducting metal chalcogenides of the stibnite family. An emphasis is placed on convergence tests and on the sensitivity of the quasiparticle corrections to the structural parameters, the inclusion of semicore d states in the calculations, and relativistic effects.

Our calculated band gaps are 1.5 eV (Sb_2S_3), 1.3 eV (Sb_2Se_3), 1.4 eV (Bi_2S_3), and 0.9 eV (Bi_2Se_3). By inspection of the band structures we infer that all four compounds have direct band gaps, although in most cases an indirect transition just below the direct gap (within 0.1 eV) is also possible. The inclusion of semicore electrons in the calculations is found to modify the band gaps by 0.1–0.2 eV. In addition we find that the gaps are rather sensitive to the lattice parameters, as they change by up to 0.3 eV when the lattice parameters are taken from experiment or fully optimized within DFT. Relativistic corrections are found to be essentially negligible for Sb_2S_3 and Sb_2Se_3, while in the case of Bi_2S_3 and Bi_2Se_3 the band gaps decrease by 0.3–0.4 eV upon inclusion of spin-orbit coupling.

The paper is organized as follows. In Sec. II we describe the computational methodology and the convergence tests for the *GW* calculations. In Sec. III we present our main results, including quasiparticle band structures and band gaps. In Sec. IV we discuss our findings in relation to the photovoltaics applications of the materials considered in this work. In Sec. V we summarize our results and present our conclusions.

II. METHODOLOGY

A. DFT calculations

All DFT calculations are performed using the QUANTUM ESPRESSO package.[46] The calculations are based on the local density approximation (LDA) to DFT.[47,48]

Only valence electrons are explicitly described, and the core-valence interaction is taken into account by means of Troullier-Martins scalar relativistic pseudopotentials[49] generated using the FHI98 code.[50] In the cases of S (Se) the $3s^23p^4$ ($4s^24p^4$) electrons are included in the valence as usual. For Sb and Bi we generate two sets of pseudopotentials, one set with five electrons in the valence, i.e., $5s^25p^3$ and $6s^26p^3$, respectively, and one set with additional semicore $4d^{10}$ and $5d^{10}$ electrons, respectively.

The electronic wave functions are expanded in plane-wave basis sets with kinetic energy cutoffs of 70 Ry (Sb_2Se_3, Bi_2Se_3) and 90 Ry (Sb_2S_3, Bi_2S_3) for the calculations without semicore states, and 100 Ry (Bi_2S_3, Bi_2Se_3) and 130 Ry (Sb_2S_3, Sb_2Se_3) when semicore states are included. In each case considered the selected cutoff yields a total energy converged to within 2 meV/atom. All self-consistent calculations are carried out using a $8 \times 8 \times 8$ Brillouin zone mesh centered at Γ, corresponding to 170 irreducible points for Sb_2S_3 and Bi_2S_3, and 260 points for Sb_2Se_3 and Bi_2Se_3.

We perform full geometry optimizations of the lattice parameters and the atomic positions in each case, both with or without semicore d states. All structural optimizations are performed using $4 \times 8 \times 4$ Γ-centered Brillouin zone meshes.

B. Crystal structure

Stibnite (Sb_2S_3), antimonselite (Sb_2Se_3), bismuthinite (Bi_2S_3), and guanajuatite (Bi_2Se_3) all crystallize in the same orthorhombic lattice and belong to the *Pnma* 62 space group.[36] Each unit cell contains 20 atoms, whose coordinates can be generated by applying the symmetry operations of the crystallographic group to a set of 5 atomic coordinates. Figure 1 shows a ball-and-stick representation of these A_2B_3 structures. The structural parameters were measured in Refs. 27 and 51–53 and are reported in Ref. 36.

As the crystal structure consists of a bundle of relatively well separated ribbons, it is convenient to separate the cohesive energy into intra-ribbon and inter-ribbon components. The intra-ribbon cohesive energy is calculated as the difference between the total energy of one ribbon and the total energies of its constituent atoms. The inter-ribbon cohesive energy is evaluated as the difference between the total energy of the unit cell and twice the total energy of one ribbon in isolation (each unit cell contains two ribbons).

C. Quasiparticle calculations

We calculate the quasiparticle energies within many-body perturbation theory using the *GW* method,[44,54–57] as implemented in the SAX code.[58] The *GW* self-energy is evaluated in the G_0W_0 approximation as $\Sigma = iG_0W_0$. Here G_0 denotes

the electron Green's function defined by the Kohn-Sham eigenstates $\psi_{n\mathbf{k}}(\mathbf{r})$ and eigenvalues $\epsilon_{n\mathbf{k}}$ corresponding to the band index n and the wave vector $\mathbf{k}$, and W_0 represents the screened Coulomb interaction calculated in the random phase approximation.[54,59] The quasiparticle energies $E_{n\mathbf{k}}$ are obtained as[54]

$$E_{n\mathbf{k}} = \epsilon_{n\mathbf{k}} + Z_{n\mathbf{k}}\langle\psi_{n\mathbf{k}}|\Sigma(\epsilon_{n\mathbf{k}}) - V_{xc}|\psi_{n\mathbf{k}}\rangle, \quad (1)$$

where $E_{n\mathbf{k}}$ is the quasiparticle energy, $Z_{n\mathbf{k}}$ is the associated quasiparticle renormalization, and V_{xc} is the exchange and correlation potential.

The self-energy can be written as the sum of a bare exchange contribution Σ_x and a correlation contribution Σ_c: $\Sigma = \Sigma_x + \Sigma_c$. The exchange part does not depend explicitly on the excitation energy and reads[60]

$$\Sigma_x(\mathbf{r},\mathbf{r}') = -\sum_{n\in\mathrm{occ},\mathbf{k}} \psi^*_{n\mathbf{k}}(\mathbf{r})\psi_{n\mathbf{k}}(\mathbf{r}')v(\mathbf{r},\mathbf{r}'), \quad (2)$$

where the sum is over occupied states and v represents the bare Coulomb interaction. This contribution to the quasiparticle correction is sensitive to the overlap between Kohn-Sham wave functions regardless of their energy. As a result the use of semicore states can have significant effect on the calculations, as shown in Refs. 61–63. This aspect will be discussed in detail in Sec. III C.

The energy dependence of the correlation contribution Σ_c arising from the dynamically screened Coulomb interaction is described via the Godby-Needs plasmon-pole model.[64] We use a plasmon-pole energy of 1 Ry for all materials, similar to the energy of the peaks in the calculated electron energy loss spectra.

Since the computational efforts for achieving convergence in Σ_c and Σ_x are very different owing to the necessity of evaluating unoccupied states for Σ_c, we perform separate convergence tests for these two components. For the exchange contribution we use kinetic energy cutoffs of 75 Ry and 100 Ry for calculations without and with semicore electrons, respectively. For the correlation contribution we perform convergence tests by calculating the band gap at various kinetic energy cutoffs up to 7 Ry for the polarizability. Figure 2(a) shows that the band gap is converged within 0.05 eV already for a cutoff of 5 Ry. The dependence of the band gap on the polarizability cutoff shows the same trend for calculations with or without semicore states. This is consistent with the expectation that the effect of semicore states in Σ_c should be small.[61] Based on the data of Fig. 2(a), in the following we use a polarizability cutoff of 7 Ry for calculations without semicore electrons, and of 6 Ry for the more demanding calculations including semicore states. In Fig. 2(b) we show the convergence of the band gap of antimonselite with respect to the energy of the highest unoccupied state included in the polarizability. Based on the trend in this figure we set the number of unoccupied states to 224 and 264 for calculations with and without semicore, corresponding to a maximum energy denominator of 35 eV. Both G_0 and W_0 are calculated on uniform and Γ-centered $2 \times 6 \times 2$ Brillouin-zone meshes.

In order to estimate the accuracy of our quasiparticle corrections with respect to the above convergence parameters we follow the approach of Ref. 65. In this approach the dependence of the band gap on a given convergence parameter is fitted by a simple function in order to extract a "best-guess" asymptotic limit. This asymptotic limit is then taken to represent the converged gap. In this work we tentatively approximate gap vs cutoff curves using the following function:

$$E^{\mathrm{QP}}_{\mathrm{gap}} = a_0 + a_1(x - a_2)^{-1/a_3}, \quad (3)$$

where $E^{\mathrm{QP}}_{\mathrm{gap}}$ is the quasiparticle band gap, x is the convergence parameter (i.e., the polarizability cutoff or the largest energy denominator), and $a_0, \ldots, a_3$ are fitting parameters. While Eq. (3) is largely arbitrary, this choice reflects the expectation that the gap will converge faster than $1/x$ owing to the damping introduced by the matrix elements in the Adler-Wiser polarizability.[66,67] Figure 2 shows that the fitting curves obtained for stibnite describe rather accurately the calculated data points; therefore it is reasonable to assume that the parameter a_0 obtained from the fit should provide a good estimate of the converged gap. By repeating this procedure for

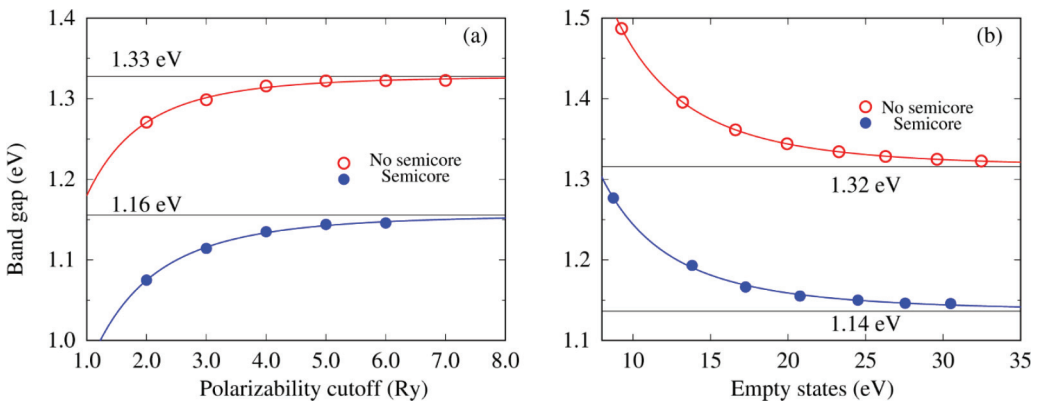

FIG. 2. (Color online) Convergence tests for the quasiparticle band gap of antimonselite. (a) Calculated G_0W_0 band gap as a function of the polarizability cutoff, for calculations without (red circles) or with (blue disks) semicore states. The solid lines correspond to the fits obtained from Eq. (3). We find $a_0 = 1.33$ eV and 1.16 eV for calculations without and with semicore electrons, respectively. (b) Same as in (a), with the band gap reported as a function of the largest energy denominator used for calculating the polarizability. In this case we find $a_0 = 1.32/1.14$ eV for calculations without/with semicore electrons. All calculations were performed using optimized lattice parameters.

all four compounds Sb_2S_3, Sb_2Se_3, Bi_2S_3, and Bi_2Se_3 we find that the convergence parameters described above yield band gaps which differ by less than 0.05 eV from the corresponding asymptotic values.

D. Spin-orbit coupling

Owing to the high atomic numbers of Bi and Sb, it is important to check the role of spin-orbit coupling (SOC) in the electronic structure of semiconductors of the stibnite family. In this work we evaluate SOC effects at the DFT level, by constructing a set of fully relativistic Troullier-Martins pseudopotentials including semicore d states. The pseudopotentials are generated using the LD1.X program of the QUANTUM ESPRESSO package. We checked that the plane-wave cutoffs described in Sec. II A for scalar-relativistic calculations are also appropriate for these fully relativistic pseudopotentials. For S and Se relativistic effects are not expected to be significant, and scalar-relativistic pseudopotentials are used throughout. We determine the spin-orbit corrections to the band gaps by taking the differences between self-consistent calculations using the fully relativistic pseudopotentials with or without noncollinear magnetism.[68] We then apply these differences as scissor corrections to the corresponding quasiparticle band gaps obtained from scalar relativistic calculations.

III. RESULTS

A. Structural parameters

Table I shows the comparison between our calculated lattice parameters and experiment. As expected the use of the local density approximation leads to a general underestimation of the experimental parameters. Interestingly, while such underestimation does not exceed 1.1% along the direction of the $(A_4B_6)_n$ ribbons (b parameter in Table I; cf. Fig. 1), the deviation can reach up to 4.2% in the direction perpendicular to the ribbons (a and c parameters in Table I). We tentatively assign this behavior to the fact that inter-ribbon forces are likely to include nonnegligible van der Waals components, and hence are not described correctly within the LDA.

Inspection of the calculated cohesive energies seems to support this possibility. Indeed we obtain intra-ribbon cohesive energies of 3.9 eV/atom (Sb_2S_3), 3.5 eV/atom (Sb_2Se_3), 3.6 eV/atom (Bi_2S_3), and 3.3 eV/atom (Bi_2Se_3). The inter-ribbon cohesive energies are one order of magnitude smaller, 0.2 eV/atom (Sb_2S_3 and Sb_2Se_3) and 0.3 eV/atom (Bi_2S_3 and Bi_2Se_3).

We also performed additional calculations of the structural parameters using the van der Waals functional of Ref. 69. The lattice parameters calculated using the vdW functional overestimate the experimental values by up to 6.9% along the directions perpendicular to the ribbons, while along the ribbons the calculated parameters are in agreement with experiment (within 0.3%). Similar trends have been observed in calculations on graphite and boron nitride in Ref. 70. These results indicate that for semiconductors of the stibnite family the use of a van der Waals functional does not improve the agreement of the calculated structural parameters with experiment.

In order to take into account the differences between calculated and experimental lattice parameters, in the following we report quasiparticle calculations obtained using either the DFT/LDA structure or the experimental structure.

B. DFT/LDA band structures

Figure 3 shows the DFT/LDA band structures calculated using experimental lattice parameters and without semicore electrons. Calculations including the semicore states yield very similar band structures. For clarity we only show the dispersions along the Z-Γ-X path and along the Y-Γ segment running along the axis of the $(A_4B_6)_n$ ribbons. The top of the valence band is found to be predominantly of S-3p or Se-4p character, while the bottom of the conduction band comprises Sb-5p or Bi-6p states, consistently with previous calculations.[36,42]

The band structures shown in Fig. 3 exhibit several extrema in proximity of the fundamental gap, making the direct and indirect transitions almost degenerate. Table II shows that the energy separation between direct and indirect DFT/LDA band gaps falls within 0.15 eV in all cases. The data in the

TABLE I. Comparison between the calculated DFT/LDA lattice parameters of stibnite, antimonselite, bismuthinite, and guanajuatite and experiment (all values are given in Å). The percentile deviation from experiment is indicated in each case.

	Experiment			Calc. w/o semicore			Calc. with semicore		
	a	b	c	a	b	c	a	b	c
Sb_2S_3	11.311[a]	3.836[a]	11.229[a]	11.036	3.795	10.753	11.087	3.838	10.834
				−2.4%	−1.1%	−4.2%	−2.0%	0.1%	−3.5%
Sb_2Se_3	11.794[b]	3.986[b]	11.648[b]	11.609	3.952	11.213	11.646	3.989	11.287
				−1.6%	−0.9%	−3.7%	−1.3%	0.1%	−3.1%
Bi_2S_3	11.305[c]	3.981[c]	11.147[c]	11.227	3.999	11.001	11.030	3.949	10.853
				−0.7%	0.5%	−1.3%	−2.4%	−0.8%	−2.6%
Bi_2Se_3	11.830[d]	4.090[d]	11.620[d]	11.767	4.141	11.491	11.609	4.099	11.374
				−0.5%	1.3%	−1.1%	−1.9%	0.2%	−2.1%

[a]Reference 51.
[b]Reference 52.
[c]Reference 53.
[d]Reference 27.

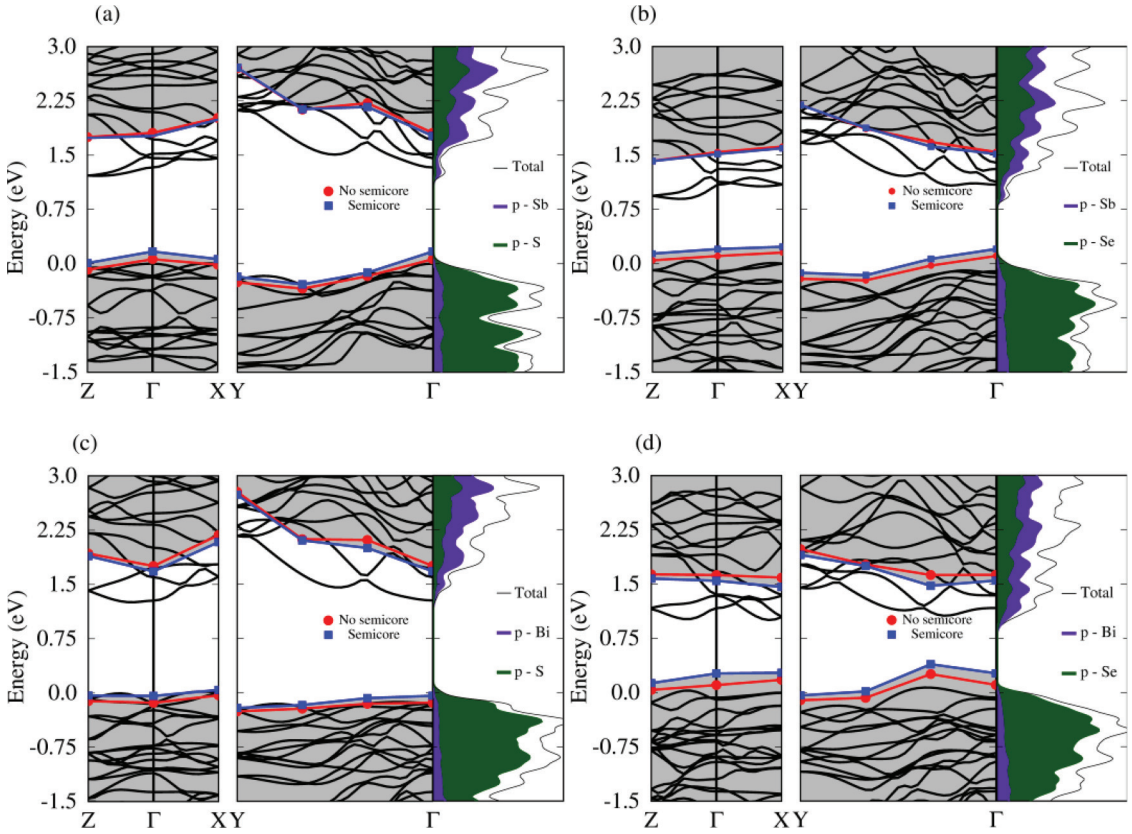

FIG. 3. (Color online) Band structures of (a) stibnite, (b) antimonselite, (c) bismuthinite, and (d) guanajuatite calculated using DFT/LDA, experimental lattice parameters, and without semicore electrons (black solid lines), as well as corresponding density of states (DOS, black dashed lines). The contributions to the DOS from the p states of S and Se (Sb and Bi) are indicated by the green (blue) shaded areas in each case. The *GW* quasiparticle energies of the band extrema at high-symmetry points are also shown, with blue squares and red circles indicating calculations with or without semicore electrons, respectively. The connecting lines are guides to the eye. The coordinates of the high-symmetry points in reciprocal lattice units are as follows: Z: (0,0,0.5), X: (0.5,0,0), Y: (0,0.5,0).

table suggest that in these compounds the direct transition will most likely dominate over the indirect one, apart from a very narrow onset of 0.1–0.2 eV. This observation is consistent with experimental evidence showing a weak absorption onset just below the threshold for direct absorption.[11,30] Therefore for practical purposes, and in particular for photovoltaics applications, stibnite, antimonselite, bismuthinite, and guanajuatite can be considered as "effectively direct gap" semiconductors.

TABLE II. Comparison between the minimum band gaps and the direct band gaps of stibnite, antimonselite, bismuthinite, and guanajuatite, as obtained from DFT/LDA. In these calculations we use the experimental lattice parameters. All values are in units of eV.

	Mimimum gap		Direct gap	
	w semicore	w/o semicore	w semicore	w/o semicore
Sb_2S_3	1.19	1.21	1.26	1.27
Sb_2Se_3	0.84	0.86	0.84	0.86
Bi_2S_3	1.25	1.24	1.28	1.27
Bi_2Se_3	0.85	0.86	0.99	0.99

C. Quasiparticle corrections

Figure 3 shows that *GW* quasiparticle corrections lead to a moderate increase of the band gaps in all cases, while generally preserving the shape of the band extrema. From this figure we deduce that a simple scissor operator should be able to capture the most important effects of the *GW* corrections.

A detailed analysis of the quasiparticle corrections at the high-symmetry points Γ, X, and Z is given in Fig. 4 and Table III. In Fig. 4 we report the quasiparticle corrections as a function of the corresponding Kohn-Sham eigenvalues around the band extrema. In the cases of stibnite and antimonselite we observe that in the calculations with semicore electrons the valence bands are slightly upshifted (by about 0.1 eV) as compared to calculations without semicore, while the corrections to the conduction bands are essentially the same. In the cases of bismuthinite and guanajuatite the effect of semicore is to shift the valence bands up and the conduction bands down by a similar amount (∼0.1 eV). As a result of these small changes, the quasiparticle corrections to the band gaps calculated with or without semicore electrons can differ by up to 0.2 eV (cf. Table III).

Semicore electrons appear to slightly reduce the quasiparticle corrections as compared to calculations without the semicore. This finding is consistent with previous calculations

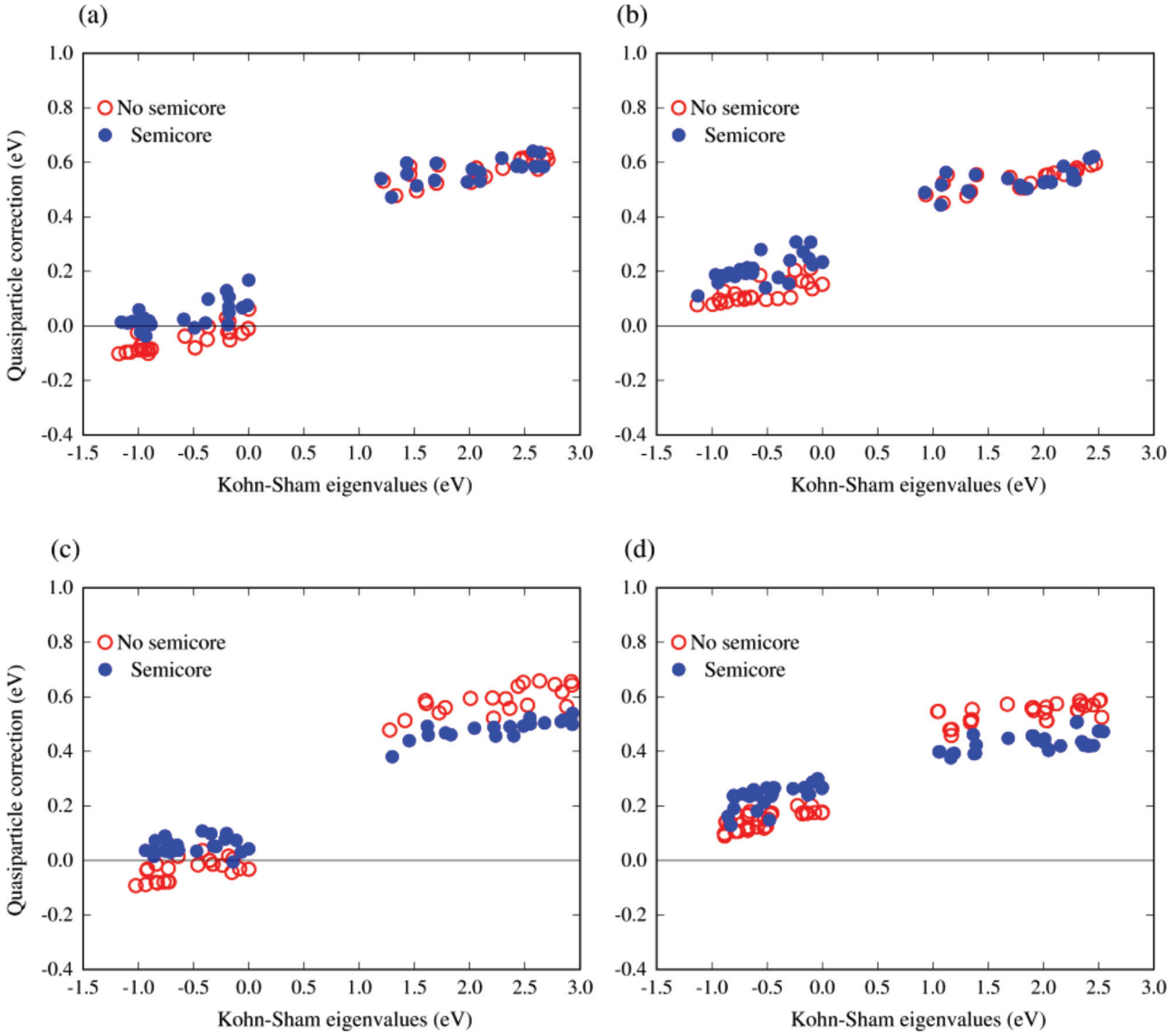

FIG. 4. (Color online) Quasiparticle corrections as a function of the corresponding DFT/LDA eigenvalues for (a) stibnite, (b) antimonselite, (c) bismuthinite, and (d) guanajuatite. Only eigenvalues at the high-symmetry points Γ, X, and Z are considered. Blue disks and red circles indicate calculations with and without semicore electrons, respectively. All calculations were performed using experimental lattice parameters.

and can be rationalized as follows.[61–63] The semicore d states introduce additional contributions Σ_x^{SC} and Σ_c^{SC} to the GW self-energy. Of these contributions, while the correlation part Σ_c^{SC} is small owing to the large energy separation between semicore states and conduction states, the exchange part Σ_x^{SC} can be large since it does not contain energy denominators but is sensitive to the overlap between the band edge states and the semicore states. This interpretation is confirmed by Fig. 5, where we can see that the inclusion of semicore electrons does indeed affect the exchange part of the GW corrections, while at the same time the correlation component remains almost unchanged.

Table III reports the DFT/LDA eigenvalues and the corresponding quasiparticle corrections for the valence band top and conduction band bottom at the high-symmetry points Γ, X, and Z. From this table we see that the LDA band gaps at these points are sensitive to the choice of the lattice parameters, and this sensitivity is reflected in the corresponding quasiparticle energies. Calculations performed using optimized lattice parameters or experimental parameters can differ by up to 0.3 eV. This observation may explain the lack of consensus between previous computational investigations of the band structures of these compounds.[8,36,39,43]

Taken together the sensitivity of the quasiparticle energies to the presence of semicore electrons and to the choice of lattice parameters leads to nonnegligible variations in the calculated band gaps. This suggests that it is important to use some care when comparing the quasiparticle band structures of stibnite and related compounds with experimental data.

In the remainder of this paper we will focus on calculations using experimental lattice parameters and including semicore

TABLE III. Quasiparticle energies of stibnite, antimonselite, bismuthinite, and guanajuatite at the high-symmetry points Γ, X, Z vs the corresponding DFT/LDA eigenvalues. We report both sets of results obtained using optimized or experimental lattice parameters. The columns labeled "S" and "w/o S" indicate calculations with and without semicore electrons, respectively. For each high-symmetry point we consider the energies at the valence band top (e.g., Γ_v) and the conduction band bottom (e.g., Γ_c). All values are in units of eV.

	Optimized parameters				Expt. parameters			
	LDA		GW		LDA		GW	
	w/o S	S	w/o S	S	w/o S	S	w/o S	S
				Stibnite				
Γ_v	0.00	0.00	0.10	0.20	0.00	0.00	0.06	0.17
Γ_c	1.15	1.11	1.58	1.52	1.33	1.29	1.81	1.77
X_v	−0.05	−0.03	−0.03	0.09	0.00	−0.01	−0.02	0.06
X_c	1.40	1.39	1.90	1.88	1.46	1.43	2.01	1.99
Z_v	−0.16	−0.14	−0.14	−0.04	−0.06	−0.06	−0.08	0.01
Z_c	1.17	1.17	1.65	1.65	1.22	1.20	1.75	1.74
				Antimonselite				
Γ_v	−0.12	−0.12	0.07	0.18	−0.11	−0.11	0.11	0.20
Γ_c	0.97	0.91	1.40	1.32	1.09	1.07	1.54	1.52
X_v	0.00	0.00	0.19	0.29	0.00	0.00	0.15	0.23
X_c	1.05	1.00	1.53	1.46	1.10	1.08	1.62	1.60
Z_v	−0.23	−0.24	−0.06	0.02	−0.09	−0.09	0.04	0.14
Z_c	0.92	0.91	1.37	1.35	0.94	0.93	1.42	1.42
				Bismuthinite				
Γ_v	−0.10	−0.04	−0.04	0.08	−0.14	−0.12	−0.14	−0.04
Γ_c	1.14	1.14	1.57	1.48	1.28	1.30	1.76	1.68
X_v	0.00	0.00	0.02	0.09	0.00	0.00	−0.03	0.04
X_c	1.50	1.67	2.04	2.09	1.61	1.63	2.18	2.09
Z_v	−0.15	−0.11	−0.13	−0.04	−0.08	−0.07	−0.11	−0.04
Z_c	1.43	1.51	1.89	1.93	1.41	1.45	1.93	1.89
				Guanajuatite				
Γ_v	−0.02	−0.02	0.18	0.30	−0.07	−0.04	0.11	0.26
Γ_c	0.95	0.89	1.39	1.24	1.17	1.16	1.63	1.54
X_v	0.00	0.00	0.19	0.28	0.00	0.00	0.18	0.27
X_c	1.07	1.18	1.61	1.58	1.04	1.06	1.59	1.45
Z_v	−0.24	−0.19	−0.06	0.05	−0.14	−0.12	0.04	0.12
Z_c	1.17	1.25	1.63	1.65	1.16	1.18	1.64	1.57

electrons, which we consider our best estimates for the quasiparticle energies in these compounds.

D. Relativistic corrections

We calculate the relativistic corrections within DFT/LDA for all four structures using the experimental structure. The corrections to the band edges at the high-symmetry points Γ, X, and Z are reported in Table IV.

In all four semiconductors the inclusion of spin-orbit coupling does not alter the top of the valence band. This is consistent with the observation that the states at the valence band top are predominantly associated with S or Se p states. On the other hand the bottom of the conduction bands are of Bi or Sb p character (see Fig. 3); hence a spin-orbit splitting is expected in this case. We calculate indeed a very small spin-orbit splitting for Sb_2S_3 and Sb_2Se_3, which has the effect of lowering the conduction band minima by less than 0.1 eV. In the case of Bi_2S_3 and Bi_2Se_3 the spin-orbit splitting is as large as 0.3–0.4 eV, consistent with the higher atomic number of Bi.

E. Band gaps

Table V reports the quasiparticle band gaps calculated using the experimental structures, including semicore electrons and relativistic corrections. The band gaps are obtained by considering the band extrema at Γ, X, and Z and we give both the fundamental gap and the direct gap. While in antimonselite and bismuthinite the calculated minimum gap is indirect, the difference between direct and indirect gaps is within 0.1 eV. In guanajuatite and stibnite the fundamental gap is direct. These results suggest that all four compounds can be considered direct-gap semiconductors for practical applications, especially in the area of optoelectronics. The calculated direct gaps are 1.54 eV (stibnite), 1.27 eV (antimonselite), 1.42 eV (bismuthinite), and 0.91 eV (guanajuatite). As shown in Table V these values are in line with previous *GW* calculations where available,[37,43] and also rather close to measured optical gaps.

The comparison with experimental data is not straightforward since the experimental literature appears to only report optical gaps (cf. literature review in Table V). However our calculations refer to quasiparticle gaps and do not include excitonic effects. Including excitonic effects using the

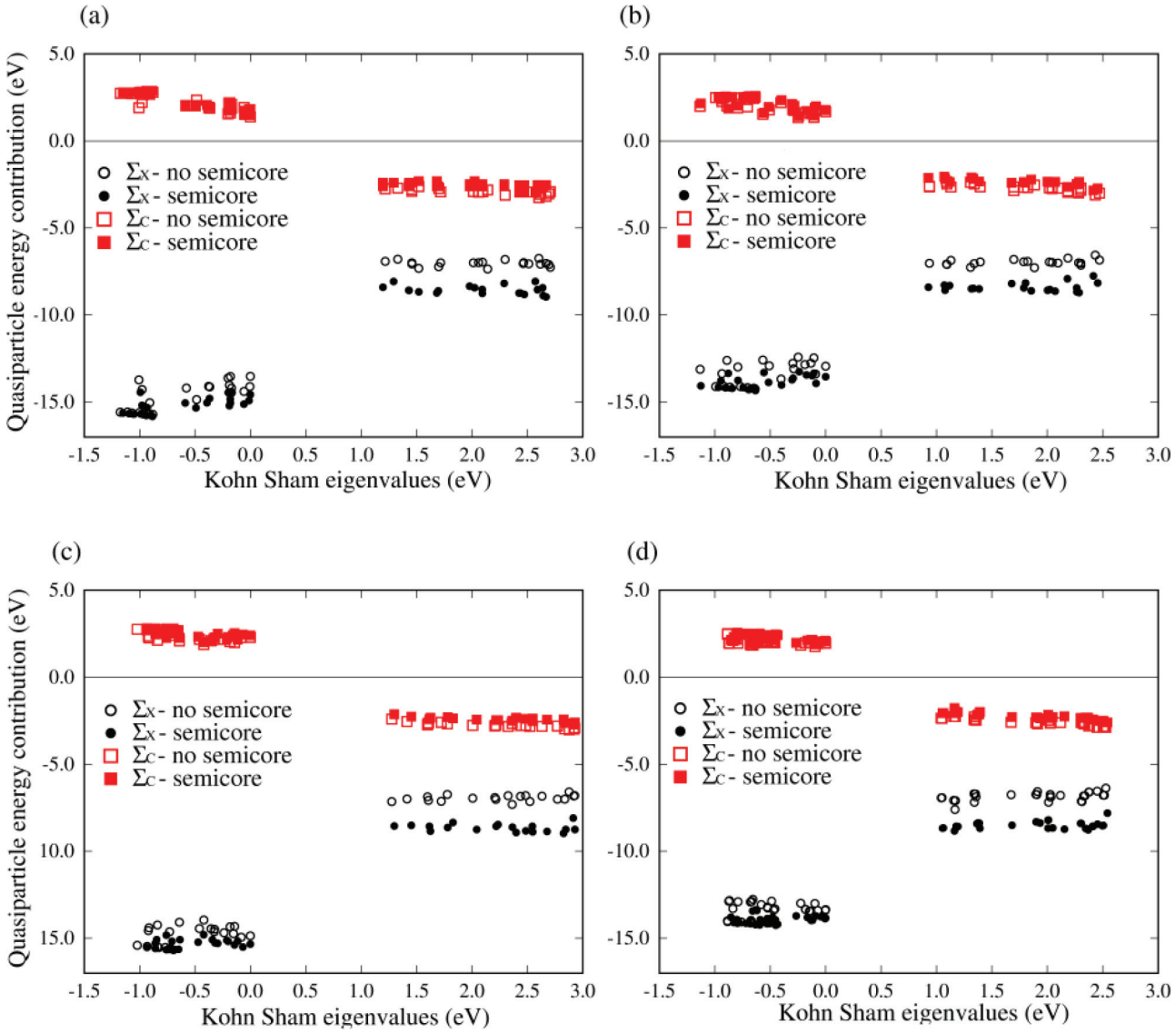

FIG. 5. (Color online) Exchange (black disks and circles) and correlation (red filled and empty squares) contributions to the quasiparticle corrections vs DFT/LDA eigenvalues for (a) stibnite, (b) antimonselite, (c) bismuthinite, and (d) guanajuatite. Only eigenvalues at the high-symmetry points Γ, X, and Z are considered. Filled and empty symbols indicate calculations with and without semicore states, respectively. All calculations were performed using experimental lattice parameters.

TABLE IV. Relativistic corrections calculated for stibnite, antimonselite, bismuthinite, and guanajuatite at high-symmetry points. The column labeled "w/o SOC" indicates the scalar relativistic values of the band edges, while the column labeled "SOC" reports the corresponding relativistic corrections. All calculations are performed using the experimental structures and including semicore d states. All values are in units of eV.

	Sb_2S_3		Sb_2Se_3		Bi_2S_3		Bi_2Se_3	
	w/o SOC	SOC	w/o SOC	SOC	w/o SOC	SOC	w/o SOC	SOC
Γ_v	0.00	0.00	−0.11	0.00	−0.12	−0.02	−0.04	−0.01
Γ_c	1.29	−0.06	1.07	−0.05	1.30	−0.32	1.16	−0.38
X_v	−0.01	0.00	0.00	0.00	0.00	−0.02	0.00	−0.02
X_c	1.43	−0.04	1.08	−0.03	1.63	−0.40	1.06	−0.27
Z_v	−0.06	0.00	−0.09	0.00	−0.07	−0.02	−0.12	−0.01
Z_c	1.20	−0.02	0.93	−0.02	1.45	−0.31	1.18	−0.28

TABLE V. Comparison between calculated and measured band gaps of stibnite, antimonselite, bismuthinite, and guanajuatite. We report the direct band gaps calculated within DFT/LDA and *GW* after the SOC corrections, as well as the measured optical gaps. The direct gaps are reported for the Γ point. The values in parentheses indicate the calculated indirect band gaps in each case. All values are in units of eV. Our calculations include semicore electrons and are performed using the experimental structures.

	Previous DFT	Present DFT + SOC	Previous *GW*	Present *GW* + SOC	Experiment
Sb_2S_3	1.55[a], 1.76[b], 1.3[c], 1.18[d], 1.22[e]	1.23	1.67[e]	1.54	1.73[f], 1.42–1.65[g], 1.78[h], 1.7[i], 1.74[j]
Sb_2Se_3	1.14[a], 0.99[d], 0.79[k], 0.89[e]	1.13 (0.91)	1.21[k]	1.27 (1.17)	1.55[l], 1.2[i], 1.0–1.2[m]
Bi_2S_3	1.47[a], 1.32[n], 1.63[n], 1.45[n], 1.67[n]	1.12 (1.00)		1.42 (1.34)	1.4[o], 1.38[p], 1.58[q],[j]
Bi_2Se_3	0.9[a], 1.1[r]	0.83		0.91	

[a]Reference 36.
[b]Reference 42.
[c]Reference 8.
[d]Reference 39.
[e]Reference 43.
[f]Reference 11.
[g]Reference 29.
[h]Reference 30.
[i]Reference 71.
[j]Reference 35.
[k]Reference 37.
[l]Reference 31.
[m]Reference 32.
[n]Reference 41.
[o]Reference 72.
[p]Reference 33.
[q]Reference 34.
[r]Reference 40.

Bethe-Salpeter approach[57] would be rather challenging owing to the large size of these systems. To the best of our knowledge no excitonic effects were measured or mentioned for any of the four compounds studied. One exception is possibly the absorption spectrum reported in Ref. 11, which exhibits some sharp features resembling excitonic peaks; however the authors assigned those peaks to defects or internal reflections. The agreement between our calculated quasiparticle gaps and the measured optical gaps can be seen *a posteriori* as an indication that excitonic shifts are small in this class of semiconductors.

Figure 6 provides a schematic view of our final calculated band gaps (*GW* + SOC) compared to the Kohn-Sham band gaps (DFT/LDA + SOC) and experiment.

IV. DISCUSSION

Taking the calculated quasiparticle band gaps of 0.9–1.5 eV as representative of the optical gaps, the four semiconductors considered here lie precisely in the range of the optimal Shockley-Queisser performance.[73] The Shockley-Queisser analysis addresses the ultimate efficiency of a solar cell based on a single material as light absorber and electron conductor, e.g. silicon solar cells. In this analysis the optimum efficiency results from a trade-off between maximizing the band gap in order to increase the photovoltage, and minimizing the band gap in order to increase the photocurrent.[73]

In the case of nanostructured solar cells based on the donor/acceptor concept such as for instance semiconductor-sensitized solar cells,[1,7] the Shockley-Queisser analysis needs to be modified in order to take into account the energy-level alignment at the donor/acceptor interface. In fact, while the photocurrent is still determined by the optical gap of the absorber (typically the donor), at variance with conventional bulk solar cells, the photovoltage is dictated by

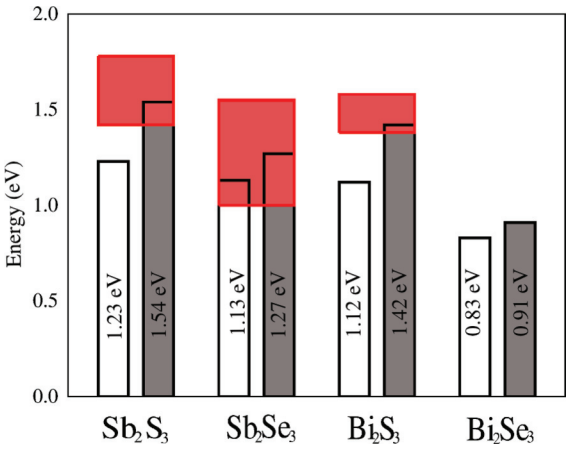

FIG. 6. (Color online) Schematic summary of the band gaps of stibnite, antimonselite, bismuthinite, and guanajuatite calculated in this work: Kohn-Sham gaps (empty rectangles) and *GW* gaps (filled rectangles) including relativistic corrections. The band gaps were obtained by including semicore electrons and using the experimental lattice parameters. The pink rectangles indicate the range of experimental optical gaps reported in Table V.

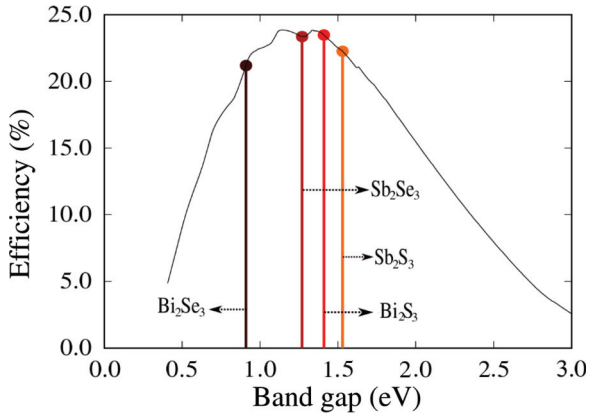

FIG. 7. (Color online) Ideal efficiency of nanostructured solar cells based on semiconductors of the stibnite family. The theoretical efficiency as a function of the band gap energy (black solid curve) is calculated using the prescription of Ref. 74 with a loss in potential of 0.3 eV and a fill factor of 73%.

the difference between the lowest unoccupied states of the acceptor and the highest occupied states of the donor. This effect can be taken into account by introducing the concept of "loss in potential,"[74] which is the reduction of the photovoltage resulting from the energy mismatch and additional losses. Losses in potential estimated for actual devices can be as large as ∼1 eV, and the most optimistic scenario would correspond to losses as small as 0.3 eV.[74] Figure 7 shows the theoretical efficiency of semiconductor-sensitized solar cells based on stibnite, antimonselite, bismuthinite, and guanajuatite, calculated using the prescription of Ref. 74 for a loss in potential of 0.3 eV. While these estimates are very crude and the projections are possibly too optimistic, it is interesting to note that all of these four materials cluster very near the optimum power conversion efficiency of 20%–25%.

From Fig. 7 we infer that the four compounds studied here are all promising candidates for nanostructured photovoltaic applications, with antimonselite and bismuthinite slightly superior to stibnite. In particular it cannot be excluded that guanajuatite, even if unstable at room temperature in bulk form, could be stabilized as a nanostructure. Given its projected maximum efficiency in Fig. 7, it might be worthwhile to attempt the synthesis of guanajuatite nanoparticles. In the case of bismuthinite Refs. 8 and 9 showed that this material does not work as a semiconductor sensitizer for TiO_2, owing to the incorrect energy-level alignment at the interface. However it cannot be excluded that bismuthinite could still reach the ideal efficiency when combined with an alternative acceptor, e.g., SnO_2 or ZnO.

V. CONCLUSIONS

In this work we report a systematic study of the quasiparticle band structures of the four isostructural metal chalcogenides stibnite (Sb_2S_3), antimonselite (Sb_2Se_3), bismuthinite (Bi_2S_3), and guanajuatite (Bi_2Se_3), within the *GW* approximation.

In order to ensure reproducibility of our results we have placed an emphasis on convergence tests and explored the effects of various calculation parameters, such as the role of semicore *d* electrons and lattice parameters. The inclusion of semicore electrons in the calculations is found to modify the band gaps by up to 0.2 eV, and the choice of experimental vs optimized lattice parameters can lead to differences of up to 0.3 eV in the calculated gaps. These findings indicate that some caution should be used in discussing the theoretical band gaps of these materials and in comparing with experiment. Relativistic effects are found to lower the conduction bands of all four materials. Spin-orbit coupling effects are important in Bi_2S_3 and Bi_2Se_3, where they reduce the band gaps by 0.3–0.4 eV, while they are essentially negligible for Sb_2S_3 and Sb_2Se_3.

Our calculations indicate that all four compounds have direct band gaps, barring indirect transitions marginally below the direct gap. The calculated band gaps are 1.54 eV (stibnite), 1.27 eV (antimonselite), 1.42 eV (bismuthinite), and 0.91 eV (guanajuatite). These values fall within the range of measured optical gaps, although it must be observed that there is a considerable scatter in the experimental data, possibly due to different preparation conditions.

Using a modified Shockley-Queisser analysis,[74] we estimate the ultimate performance of solar cells based on these compounds as light sensitizers. This analysis indicates that all four materials have potential for high-efficiency nanostructured solar cells. The highest theoretical efficiencies are obtained for antimonselite and bismuthinite, followed closely by stibnite and guanajuatite, the high-temperature polymorph of the topological insulator Bi_2Se_3.

Future calculations should address the optical absorption spectra of these compounds within the Bethe-Salpeter approach, in order to establish whether excitonic effects are as small as our data appear to suggest. It will be also interesting to extend the present study to the case of individual nanoribbons of these metal chalcogenides, since liquid-phase exfoliation techniques for van der Waals bonded materials are becoming increasingly popular.[75]

We hope that the present study will contribute to the ongoing research on new materials for energy applications, and stimulate further efforts to understand and exploit these fascinating and relatively unexplored compounds.

ACKNOWLEDGMENTS

This work is supported by the UK EPSRC and the ERC under EU FP7/ERC Grant No. 239578. Calculations were performed at the Oxford Supercomputing Centre. Figures rendered using XCRYSDEN.[76]

[1] J. A. Chang, J. H. Rhee, S. H. Im, Y. H. Lee, H. Kim, S. I. Seok, M. K. Nazeeruddin, and M. Grätzel, Nano Lett. **10**, 2609 (2010).
[2] J. A. Chang, S. H. Im, Y. H. Lee, H. Kim, C.-S. Lim, J. H. Heo, and S. I. Seok, Nano Lett. **12**, 1863 (2012).
[3] A. K. Rath, M. Bernechea, L. Martinez, F. P. Garcia de Arquer, J. Osmond, and G. Kostantatos, Nat. Photonics **6**, 529 (2012).
[4] N. Guijarro, T. Lutz, T. Lana-Villarreal, F. O'Mahony, R. Gomez, and S. A. Haque, J. Phys. Chem. Lett **3**, 1351 (2012).

[5]R. J. Mehta, C. Karthik, W. Jiang, B. Singh, Y. Shi, R. Siegel, T. Borca-Tasciuc, and G. Ramanath, Nano Lett. **10**, 4417 (2010).
[6]B. O'Regan and M. Grätzel, Nature (London) **353**, 737 (1991).
[7]G. Hodes, J. Phys. Chem. C **112**, 17778 (2008).
[8]C. E. Patrick and F. Giustino, Adv. Funct. Mater. **21**, 4663 (2011).
[9]T. Lutz, A. MacLachlan, A. Sudlow, J. Nelson, M. S. Hill, K. C. Molloy, and S. A. Haque, Phys. Chem. Chem. Phys. **14**, 16192 (2012).
[10]C. H. Bhosale, M. D. Uplane, P. S. Patil, and C. D. Lockhande, Thin Solid Films **248**, 137 (1994).
[11]M. Y. Versavel and J. A. Haber, Thin Solid Films **515**, 7171 (2007).
[12]C. D. Lokhande, B. R. Sankapal, R. S. Mane, H. M. Pathan, M. Muller, M. Giersig, and V. Ganesan, Appl. Surf. Sci. **193**, 1 (2002).
[13]H. Maghraoui-Meherzi, T. Ben Nasr, N. Kamoun, and M. Dachraoui, Physica B **405**, 3101 (2010).
[14]L. Cademartiri, R. Malakooti, P. G. O'Brien, S. Petrov, N. P. Kherani, and G. A. Ozin, Angew. Chem. Int. Ed. **47**, 3814 (2008).
[15]R. Malakooti, L. Cademartiri, A. Migliori, and G. A. Ozin, J. Mater. Chem. **18**, 66 (2008).
[16]S. Rühle, M. Shalom, and A. Zaban, Chem. Phys. Chem. **11**, 2290 (2010).
[17]Q. Han, S. Sun, D. Sun, J. Zhu, and X. Wang, RSC Adv. **1**, 1364 (2011).
[18]L. Cademartiri, G. Guerin, K. J. Bishop, and M. A. Winnik, J. Am. Chem. Soc. **134**, 9327 (2012).
[19]M. E. Rincon, M. Sanchez, P. J. George, A. Sanchez, and P. K. Nair, J. Solid State Chem. **136**, 167 (1998).
[20]F. Perales, G. Lifante, F. Agulló-Rueda, and C. de la Heras, J. Phys. D: Appl. Phys. **40**, 2440 (2007).
[21]H. Bao, X. Cui, C. M. Li, Q. Song, Z. Lu, and J. Guo, J. Phys. Chem. C **111**, 17131 (2007).
[22]A. G. Vedeshwar, J. Phys. III (France) **5**, 1161 (1995).
[23]A. M. Karguppikar and A. G. Vedeshwar, Phys. Lett. A **126**, 123 (1987).
[24]Z. Deng, M. Mansuripur, and A. J. Muscat, Nano Lett. **9**, 2015 (2009).
[25]J. Varghese, S. Barth, L. Keeney, R. W. Whatmore, and J. D. Holmes, Nano Lett. **12**, 868 (2012).
[26]H. Zhang, C. X. Liu, X. L. Qi, Z. Fang, and S.-C. Zhang, Nat. Phys. **5**, 438 (2009).
[27]E. Y. Atabaeva, S. A. Mashkov, and S. V. Popova, Krystallografiya **18**, 173 (1974).
[28]H. Okamoto, J. Phase Equilib. **15**, 195 (1994).
[29]S. Mahanty, J. M. Merino, and M. León, J. Vac. Sci. Technol. A **15**, 3060 (1997).
[30]I. K. El Zawawi, A. Abdel-Moez, F. S. Terra, and M. Mounir, Thin Solid Films **324**, 300 (1998).
[31]A. P. Torane, K. Y. Rajpure, and C. H. Bhosale, Mater. Chem. Phys. **61**, 219 (1999).
[32]Y. Rodriguez-Lazcano, Y. Pena, M. T. S. Nair, and P. K. Nair, Thin Solid Films **493**, 77 (2005).
[33]J. Lukose and B. Pradeep, Solid State. Commun. **78**, 535 (1991).
[34]S. Mahmoud, A. H. Eid, and H. Omar, Fizika A **6**, 111 (1997).
[35]N. S. Yesugade, C. D. Lokhande, and C. H. Bhosale, Thin Solid Films **263**, 145 (1995).
[36]R. Caracas and X. Gonze, Phys. Chem. Minerals **32**, 295 (2005).
[37]R. Vadapoo, S. Krishnan, H. Yilmaz, and C. Marin, Phys. Status Solidi B **248**, 700 (2011).
[38]P. Larson, V. A. Greanya, W. C. Tonjes, R. Liu, S. D. Mahanti, and C. G. Olson, Phys. Rev. B **65**, 085108 (2002).
[39]H. Koc, A. M. Mamedov, E. Deligoz, and H. Ozisik, Solid State Sci. **14**, 1211 (2012).
[40]Y. Sharma and P. Srivastava, AIP Conf. Proc. **1249**, 183 (2010).
[41]Y. Sharma, P. Srivastava, A. Dashora, L. Vadkhiya, M. K. Bhayani, R. Jain, A. R. Jani, and B. L. Ahuja, Solid State Sci. **14**, 241 (2012).
[42]T. Ben Nasr, H. Maghraoui-Meherzi, H. Ben Abdallah, and R. Bennaceur, Physica B **406**, 287 (2011).
[43]R. Vadapoo, S. Krishnan, H. Yilmaz, and C. Marin, Nanotechnology **22**, 175705 (2011).
[44]L. Hedin, Phys. Rev. **139**, A796 (1965).
[45]O. V. Yazyev, E. Kioupakis, J. E. Moore, and S. G. Louie, Phys. Rev. B **85**, 161101(R) (2012).
[46]P. Giannozzi *et al.*, J. Phys.: Condens. Matter. **21**, 395502 (2009).
[47]J. P. Perdew and A. Zunger, Phys. Rev. B **23**, 5048 (1981).
[48]D. M. Ceperley and B. J. Alder, Phys. Rev. Lett. **45**, 566 (1980).
[49]N. Troullier and J. L. Martins, Phys. Rev. B **43**, 1993 (1991).
[50]M. Fuchs and M. Scheffler, Comput. Phys. Commun. **119**, 67 (1999).
[51]P. Bayliss and W. Nowacki, Z. Kristallogr. **135**, 308 (1972).
[52]G. P. Voutsas, A. G. Papazoglou, and P. J. Rentzeperis, Z. Kristallogr. **171**, 261 (1985).
[53]A. S. Kanishcheva, Y. N. Mikhailov, and A. F. Trippel, Izv. Akad. Nauk. SSSR Neorganicheskie Mater. **17**, 1972 (1981).
[54]M. S. Hybertsen and S. G. Louie, Phys. Rev. B **34**, 5390 (1986).
[55]W. G. Aulbur, L. Jönsson, and J. W. Wilkins, Solid State Phys. **54**, 1 (1999).
[56]F. Aryasetiawan and O. Gunnarsson, Rep. Prog. Phys. **61**, 237 (1998).
[57]G. Onida, L. Reining, and A. Rubio, Rev. Mod. Phys **74**, 601 (2002).
[58]L. Martin-Samos and G. Bussi, Comput. Phys. Commun. **180**, 1416 (2009).
[59]L. Hedin and S. Lundqvist, Solid State Phys. **23**, 1 (1969).
[60]F. Giustino, M. L. Cohen, and S. G. Louie, Phys. Rev. B **81**, 115105 (2010).
[61]M. Rohlfing, P. Krüger, and J. Pollmann, Phys. Rev. Lett. **75**, 3489 (1995).
[62]M. L. Tiago, S. Ismail-Beigi, and S. G. Louie, Phys. Rev. B **69**, 125212 (2004).
[63]P. Umari and S. Fabris, J. Chem. Phys. **136**, 174310 (2012).
[64]R. W. Godby and R. J. Needs, Phys. Rev. Lett. **62**, 1169 (1989).
[65]S. Sharifzadeh, I. Tamblyn, P. Doak, P. T. Darancet, and J. B. Neaton, Eur. Phys. J. B **85**, 323 (2012).
[66]S. L. Adler, Phys. Rev. **126**, 413 (1962).
[67]N. Wiser, Phys. Rev. **129**, 62 (1963).
[68]T. Oda, A. Pasquarello, and R. Car, Phys. Rev. Lett. **80**, 3622 (1998).
[69]M. Dion, H. Rydberg, E. Schroder, D. C. Langreth, and B. I. Lundqvist, Phys. Rev. Lett. **92**, 246401 (2004).
[70]D. C. Langreth, M. Dion, H. Rydberg, E. Scröder, P. Hyldgaard, and B. I. Lundqvist, Int. J. Quantum Chem. **101**, 599 (2005).
[71]J. Black, E. N. Conwell, L. Sigle, and C. W. Spencer, J. Phys. Chem. Solids **2**, 240 (1957).
[72]L. Gildart, J. M. Kline, and D. M. Mattox, J. Phys. Chem. Solids **18**, 286 (1961).
[73]W. Shockley and H. J. Queisser, J. Appl. Phys. **32**, 510 (1961).
[74]H. J. Snaith, Adv. Funct. Mater. **20**, 13 (2010).
[75]J. N. Coleman *et al.*, Science **331**, 568 (2011).
[76]A. Kokalj, Comput. Mater. Sci. **28**, 155 (2003).